

Large bandwidth, highly efficient optical gratings through high index materials

Helmut Rathgen^{*1} and H. L. Offerhaus²

¹*Physics of Complex Fluids, University of Twente, The Netherlands.*

²*Optical Sciences, University of Twente, The Netherlands.*

helmut.rathgen@web.de

<http://mrcwa.sourceforge.net/>

Abstract: We analyze the diffraction characteristics of dielectric gratings that feature a high index grating layer, and devise, through rigorous numerical calculations, large bandwidth, highly efficient, high dispersion dielectric gratings in reflection, transmission, and immersed transmission geometry. A dielectric TIR grating is suggested, whose $-1dB$ spectral bandwidth is doubled as compared to its all-glass equivalent. The short wavelength diffraction efficiency is additionally improved by allowing for slanted lamella. The grating surpasses a blazed gold grating over the full octave. An immersed transmission grating is devised, whose $-1dB$ bandwidth is tripled as compared to its all-glass equivalent, and that surpasses an equivalent classical transmission grating over nearly the full octave. A transmission grating in the classical scattering geometry is suggested, that features a buried high index layer. This grating provides effectively 100% diffraction efficiency at its design wavelength, and surpasses an equivalent fused silica grating over the full octave.

© 2022 Optical Society of America

OCIS codes: (050.1950) Diffraction gratings, (050.1960) Diffraction theory.

References and links

1. J. Limpert, T. Schreiber, T. Clausnitzer, K. Zöllner, H. Fuchs, E. Kley, H. Zellmer, and A. Tünnermann, "High-power femtosecond Yb-doped fiber amplifier," *Opt. Express* **10**(14), 628–638 (2002).
2. J. Néauport, E. Journot, G. Gaborit, and P. Bouchut, "Design, optical characterization, and operation of large transmission gratings for the laser integration line and laser megajoule facilities," *Appl. Opt.* **44**(16), 3143–3152 (2005).
3. T. Clausnitzer, J. Limpert, K. Zöllner, H. Zellmer, H.-J. Fuchs, E.-B. Kley, A. Tünnermann, M. Jupe, and D. Ristau, "Highly efficient transmission gratings in fused silica for chirped-pulse amplification systems," *Appl. Opt.* **42**, 6934 (2003).
4. H. T. Nguyen, B. W. Shore, S. J. Bryan, J. A. Britten, R. D. Boyd, and M. D. Perry, "High-efficiency fused-silica transmission gratings," *Opt. Lett.* **22**(3), 142–144 (1997).
5. N. Tamura, G. Murray, R. Sharples, D. Robertson, and J. Allington-Smith, "Measurement of throughput variation across a large format volume-phase holographic grating," *Opt. Express* **13**(11), 4125–4133 (2005).
6. T. K. Rhee, T. S. Sosnowski, T. B. Norris, J. A. Arms, and W. S. Colburn, "Chirped-pulse amplification of 85-fs pulses at 250kHz with 3rd order dispersion compensation by use of holographic transmission gratings," *Opt. Lett.* **19**(19), 1550–1552 (1994).
7. I. K. Baldry, J. Bland-Hawthorn, and J. G. Robertson, "Volume Phase Holographic Gratings: Polarization Properties and Diffraction Efficiency," *Pub. Astron. Soc. Pac.* **116**, 403 (2003).
8. N. Ebizuka, K. Oka, A. Yamada, M. Watanabe, K. Shimizu, K. Kodate, M. Kawabata, T. Teranishi, K. Kawabata, and M. Iye, "Development of volume phase holographic(VPH) grism for visible to near infrared instruments of 8. 2-m Subaru Telescope," *Proc. SPIE* **4842**, 319–328 (2002).

9. James Gregory (1638–1675) used a bird feather to create diffraction, see H W Turnbull, James Gregory (1638–1675), in *The James Gregory Tercentenary Memorial Volume* (London, 1939), 5–11.
10. J. R. Marcante and D. H. Raguin, “High-efficiency, high-dispersion diffraction gratings based on total internal reflection,” *Opt. Lett.* **29**, 542 (2004).
11. S. Liu, J. Ma, C. Wei, Z. Shen, J. Huang, Y. Jin, J. Shao, and Z. Fan, “Design of high-efficiency diffraction gratings based on total internal reflection for pulse compressor,” *Opt. Commun.* **273**, 290 (2007).
12. R. Livingston and R. Krchnavek, “Grazing angle planar diffraction grating for photonic wavelength demultiplexing,” *Electronic Components and Technology Conference, 1996. Proceedings.*, 46th pp. 958–962 (1996).
13. M. G. Moharam, D. A. Pommet, E. B. Grann, and T. K. Gaylord, “Stable implementation of the rigorous coupled-wave analysis for surface-relief gratings: enhanced transmittance matrix approach,” *J. Opt. Soc. Am. A* **12**, 1077 (1995).
14. <http://mrcwa.sourceforge.net/>.
15. G. van Rossum et al., “Python Programming Language,” <http://www.python.org/>.
16. E. Anderson, Z. Bai, C. Bischof, S. Blackford, J. Demmel, J. Dongarra, J. D. Croz, A. Greenbaum, S. Hammarling, A. McKenney, and D. Sorensen, *LAPACK User's Guide*, 3rd ed. (SIAM, Philadelphia, 1999). <http://www.netlib.org/lapack/lug/>.
17. T. Clausnitzer, T. Kämpfe, E.-B. Kley, A. Tünnermann, U. Peschel, A. Tishchenko, and O. Parriaux, “An intelligible explanation of highly-efficient diffraction in deep dielectric rectangular transmission gratings,” *Opt. Express* **13**, 10,448 (2005).
18. T. Clausnitzer, T. Kämpfe, E.-B. Kley, A. Tünnermann, A. Tishchenko, and O. Parriaux, “Highly-dispersive dielectric transmission gratings with 100% diffraction efficiency,” *Opt. Express* **16**, 5577 (2008).
19. R. Petit, *Electromagnetic theory of gratings*, vol. 22 of *Topics in Current Physics* (Springer Verlag, Berlin, 1980).
20. E. D. Palik, *Handbook of optical constants of solids* (Academic Press, Orlando, 1985).
21. J. Nishii, K. Kintaka, and T. Nakazawa, “High-Efficiency Transmission Gratings Buried in a Fused-SiO₂ Glass Plate,” *Appl. Opt.* **43**(6), 1327–1330 (2004).
22. E. A. Gibson, D. M. Gaudiosi, H. C. Kapteyn, R. Jimenez, S. Kane, R. Huff, C. Durfee, and J. Squier, “Efficient reflection grisms for pulse compression and dispersion compensation of femtosecond pulses,” *Opt. Lett.* **31**, 3363 (2006).

1. Introduction

Diffraction gratings are an integral part of many modern optical systems, with applications in lasers, imaging systems and telecommunication. Recently *dielectric* gratings have attracted increasing interest. Due to their high resistance to laser induced damage paired with an unsurpassed diffraction efficiency, etched fused silica gratings have found widespread use in laser physics, for pulse compression [1, 2, 3] and wavelength control [4]. On the other hand, the development of holographic replication techniques has enabled large area volume gratings that are imprinted onto gelatine films sandwiched between two glass plates, known as volume phase holographic (VPH) gratings [5, 6]. Their sealed layout (cleanability) and large possible dimensions makes them the primary choice for the spectrographs of the recent generation of astronomical telescopes [7, 8]. Dielectric gratings are therefore of great interest.

Here, we introduce the use of high refractive index materials to dielectric gratings. Through rigorous numerical calculations, accompanied by intuitive models, we investigate a number of new grating designs – representing total internal reflection types, immersed transmission types, and classical transmission types – that are superior to the state of the art, both in terms of peak diffraction efficiency and spectral bandwidth. Emphasis is put on devising designs that are easily fabricated in practice. The paper is organized as follows. In the remainder of this introduction, we will walk through the principles of optical gratings, and optical grating design, using the fused silica TIR grating as an example. In Sec.2, we present our numerical results for the diffraction characteristics of dielectric TIR gratings based on high index materials. In Sec.3, we extend the use of high index materials to immersed dielectric gratings. We first analyzing qualitatively the challenge of designing an immersed grating that provides high dispersion, and subsequently present our numerical results on immersed gratings featuring a high index material. Finally, in Sec.4, the use of high index materials is extended to classical dielectric transmission gratings. The paper is concluded in Sec.5.

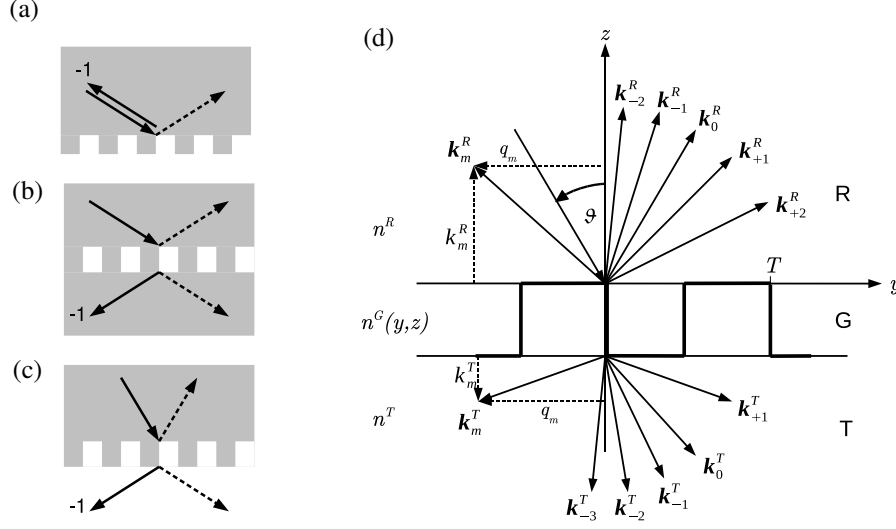


Fig. 1. (a)–(c) Schematics of the investigated types of dielectric gratings, (a) TIR grating, (b) immersed grating, (c) classical transmission grating. (d) Scattering geometry of an optical grating.

If a dielectric grating is illuminated under a sufficiently large incident angle, total internal reflection (TIR) occurs at the grating surface, and the device is turned from a transmission grating into a reflection grating. This configuration offers great benefits. Most importantly, reflection is achieved without the need of a metallic coating, and thus, the low absorption loss of the grating, and consequently a large diffraction efficiency, paired with a large resistance against laser induced damage is maintained. Given the more than 350 year long history of the optical grating [9], it is indeed remarkable, that this scattering geometry was discovered only recently [10, 11, 12].

Fig.1(a) shows the schematic of the dielectric TIR grating. Similar to an ordinary transmission grating, rectangular grooves are fabricated into the backside of a glass body, and the grating is illuminated from the glass side. However, in contrast to an ordinary transmission grating, the grating is illuminated under an incident angle that is larger than the angle of total internal reflection between glass and air ($\vartheta_T \approx 43.6^\circ$), such that the zero-order transmitted beam is evanescent. Furthermore, the period T of the grating is chosen sufficiently small, such that all other diffraction orders on the transmission side are evanescent as well. This is achieved by stressing the scattering geometry of the grating.

Fig.1(d) illustrates the scattering geometry. Generally, as an optical grating is illuminated with a plane wave, a number of plain waves are scattered from the grating. Waves are scattered into the reflection region R , and into the transmission region T , that are characterized each by their refractive index n^R , respectively n^T . Associated with every scattered wave is an amplitude and a wavevector. The wavevector expresses the direction of the wave – or, in case the wavevector is complex, the penetration depth of the evanescent wave. The components of the wavevectors in the periodic direction (here the y -components, see Fig.1) are determined by the Bloch condition as $q_m = q_0 + mQ$, where $m = -\infty, \dots, +\infty$ is the diffraction order, $Q = \lambda/T$, and $q_0 = n^R \sin \vartheta_0$. Here ϑ_0 is the incident angle. We have non-dimensionalized the spatial coordinate through $r \mapsto 2\pi r/\lambda$. The z -components of the wavevectors are determined through the wave equation as $k_m^S = (n^{S^2} - q_m^2)^{1/2}$. $S = R, T$ denotes the reflection and transmission region, respectively. A real k represents a propagating diffraction order, a complex k represents

an evanescent wave. The latter relations imply the grating equation

$$\sin \vartheta_m^S = \sin \vartheta_0^S + \frac{m\lambda}{n^S T}, \quad (1)$$

which expresses the angles of the scattered waves. Angles are measured with a positive sign in positive y -direction, and with a negative sign in negative y -direction. The angular dispersion D follows by differentiating the latter equation with respect to λ ,

$$D = \frac{\partial \vartheta_m^R}{\partial \lambda} = -\frac{m}{T n^R \cos \vartheta_m^R}. \quad (2)$$

The TIR grating is then arrived at, by requiring

$$|q_m| > n^T. \quad (3)$$

This determines a range, where the period of the grating is sufficiently small.

Generally, the highest diffraction efficiency is achieved if the grating is mounted in -1^{st} order Littrow configuration, where the -1^{st} diffraction order is antiparallel to the incident wave, that is $-q_{-1} = q_0$. To see the benefit of this, consider the opposite case: Suppose a binary (rectangular profile) reflection grating is illuminated at zero incident angle, that is, perpendicular to the surface. And suppose the period is small enough, such that only the $+1^{st}$ and the -1^{st} diffraction order are present. It is possible to choose a suitable width and depth of the grating grooves, such that the largest part of the diffracted intensity is scattered into the 0^{th} order, or, by choosing a different width and depth, all of the diffracted intensity is scattered into the first order. However, due to symmetry, the intensity of the $+1^{st}$ and the -1^{st} diffraction order must be equal, such that, at maximum 50% of the diffracted intensity is scattered into a single diffraction order. In contrast, if the incident angle is chosen such that the -1^{st} diffraction order is antiparallel to the 0^{th} order, only the 0^{th} and the -1^{st} order are present, and the scattered intensity can be distributed at will among those two orders (by choosing a suitable groove width and depth), thus (nearly) 100% diffraction efficiency can be achieved. Remarkably, near 100% diffraction efficiency can be achieved also with higher order Littrow configurations, characterized by $-q_m = q_0$, and even more surprising, this holds true even for higher order TIR gratings, where no longer all transmitted orders are forbidden (see supplemental Fig.1). This implies indeed, that the TIR grating condition can be relaxed. Rather than requiring that *all* diffraction orders on the transmission side be evanescent (as suggested originally in Ref.[10], and represented by Eq.3), it is sufficient to require that the 0^{th} transmitted order is evanescent, i.e., the ordinary condition for total internal reflection is satisfied, expressed as $|q_0| > n^T$. Independent of that, in most cases, one will design a grating for -1^{st} order Littrow configuration, because here, the overlap between higher diffraction orders is minimal – the angular range per diffraction order is largest – such that the largest spectral bandwidth can be achieved.

The Littrow configuration settles the period of the grating as

$$T = m\lambda / (2n^R \sin \vartheta_0^R). \quad (4)$$

From now on, we assume the wavelength is 1064nm, the refractive index of the glass is 1.45, and the incident angle is 60° . Thus, the period of the grating is $T = 423.66\text{nm}$ in our case. This settles also the angular dispersion, since the Littrow condition substituted in Eq.2 yields

$$D = 2/\lambda \tan \vartheta_0. \quad (5)$$

The dispersion is minimal at zero angle (perpendicular to the surface), and diverges at grazing angles. With the above parameters, the dispersion is $D = 0.187^\circ/\text{nm}$. A comparably large dispersion is inherent to TIR gratings, because of the necessarily large incident angle.

To arrive at a highly efficient TIR grating, one varies the width w and depth d of the grating grooves, and evaluates the resulting intensity of the -1^{st} diffraction order with a suitable numerical method. A number of efficient numerical methods have been developed over the past decades, that allow to do so. Here, we use the multilayer rigorous coupled wave analysis, as devised in Ref.[13]. The numerical code used in this work [14], is written in FORTRAN 90 and Python [15], and is made freely available under the GPLv3; we aim to provide a computational tool to the community, that can be openly reviewed (open source) and is free of charge. A flexible and highly intuitive user interface is provided through a set of python bindings, that are easily extended and embedded into complex computational tasks. The numerical core routines are provided by optimized FORTRAN 90 code, relying heavily on the high performance linear algebra package LAPACK [16], typically in form of the intelTMMKL. In this work, all calculations were performed on a grid equipped with 2GHz Dual Core AMD OpteronTM processors, and took only few hundred cpu hours.

The upper panel of Fig.2(a) shows the calculated diffraction intensity of the -1^{st} diffraction order as a function of groove width and depth, for s -polarized light (results for p -polarization and averaged s and p are included in the supplemental material). Broad regions appear, where the diffracted intensity is close to unity. This behavior can be understood by considering the propagation constants in normal direction, of the modes that are excited inside the grating region [17]. As the grating is arranged in -1^{st} order Littrow configuration, only the fundamental and the first mode in the grating region carry a notable amount of energy. They propagate at different velocities, determined by their propagation constants. Thus, as they propagate, they accumulate a phase shift. The phase shift that the waves have accumulated as they couple out of the grating region, determines whether they are scattered into the ordinary reflected beam or into the -1^{st} order. In this way, by choosing the depth of the grooves, the intensity can be distributed at will among the 0^{th} and the -1^{st} order. The propagation constants of the modes are determined by their effective refractive indices. Those depend on the filling fraction of the grating, that is, the groove width. Consequently, depending on the groove width, a different depth is required to achieve the desired phase difference. The fringes in Fig.2(a) correspond to integer multiples of the interference condition. It should be noted, that, along a line in the center of each fringe, the intensity is truly unity. This is in contrast to classical transmission gratings, where the maximum theoretical intensity is limited by the effective reflectivity of the grating, which inevitably results in a scattering loss into the 0^{th} order, such that 100% diffraction efficiency cannot be reached (e.g. [18], and the discussion in Sec.3, and Fig.6(a)). The latter elevates the TIR grating as a unique component for applications where highest diffraction efficiencies are required. The width-depth-map suggests a number of possible choices for the width and depth, that result in a highly efficient TIR grating. To devise a TIR grating that is easily fabricated in practice, one may chose an intermediate width and a small depth, corresponding to a small aspect ratio. The white circle in the upper panel of Fig.2(a) represents one possible choice, with $w = 0.35T$ and $d = 1.1T$. To find the spectral characteristics of the corresponding grating, one varies the wavelength of the incident light, and evaluates the resulting diffraction efficiency. The latter may be done in two ways. (1) The incident angle is held fixed, while the wavelength is varied – this case is encountered, e.g., with gratings that are used for dispersion control in femtosecond laser applications, or with spectrometers that are equipped with a line CCD and operate without movable parts. (2) As the wavelength is varied, the incident angle is adapted, such that the grating continues to satisfy the Littrow condition for every wavelength – this case is encountered, e.g., in a classical scanning monochromator. Here, we consider the first case, motivated by the application of the dielectric TIR grating for pulse compression, and furthermore, because the range of possible incident angles for the TIR grating is not particularly large.

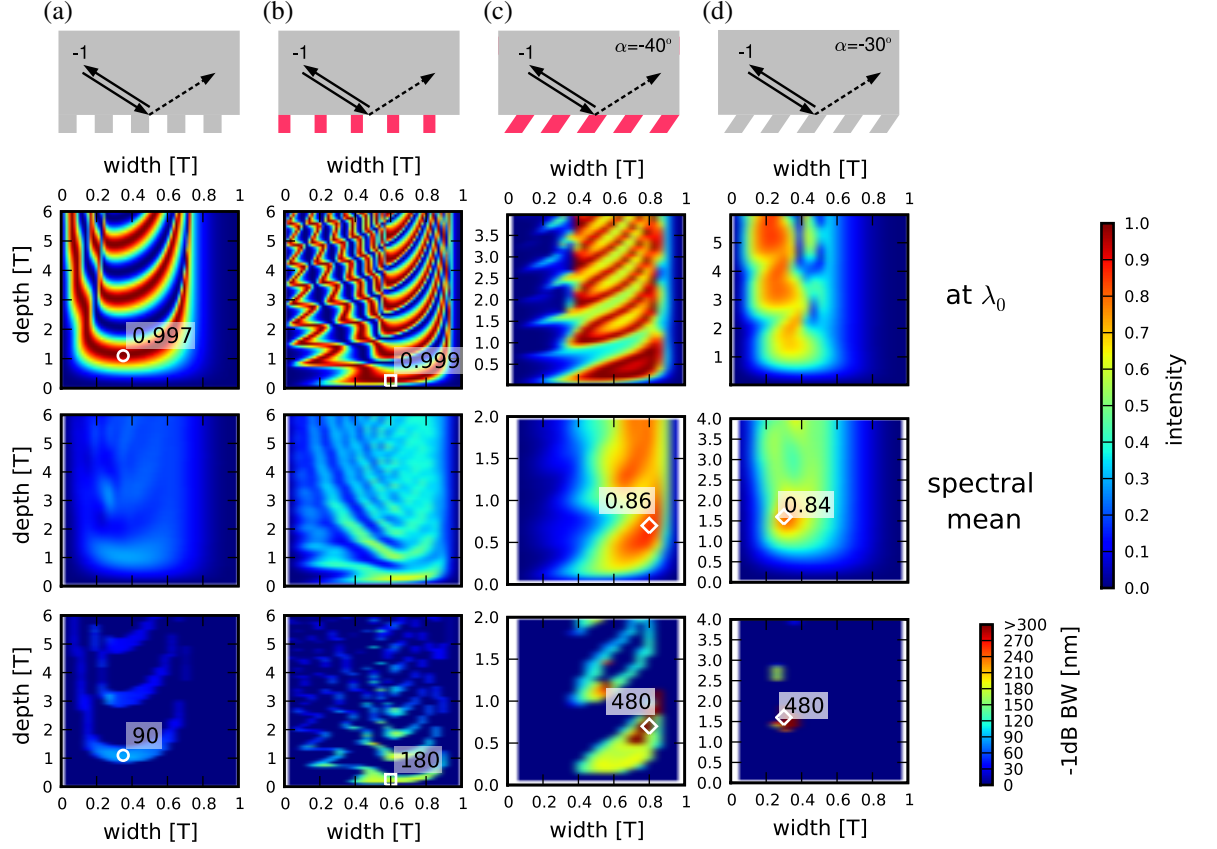


Fig. 2. Diffraction efficiency of dielectric TIR gratings as a function of the groove width and depth. (a) silica TIR grating. (b) TIR grating based on a high index material ($n=2.4$). (c) TIR grating based on a high index material featuring slanted lamella ($\alpha = 40^\circ$). (d) silica TIR grating featuring slanted lamella ($\alpha = 30^\circ$). The upper panels show the diffraction efficiency at the design wavelength $\lambda_0 = 1064\text{nm}$. The middle panels show the mean diffraction efficiency, averaged over the theoretically accessible spectral band, as determined by the condition of non-overlapping diffraction orders, $\lambda_{cut}/2 < \lambda < \lambda_{cut}$, where $\lambda_{cut} = n^R T(1 + \sin \vartheta_0)$. The lower panel shows the -1dB spectral bandwidth. The open white symbols mark optimal choices of the parameters w and d for each type of grating, and represent those values, for which the spectral characteristics is plotted in Fig.3. All results shown correspond to s -polarized light.

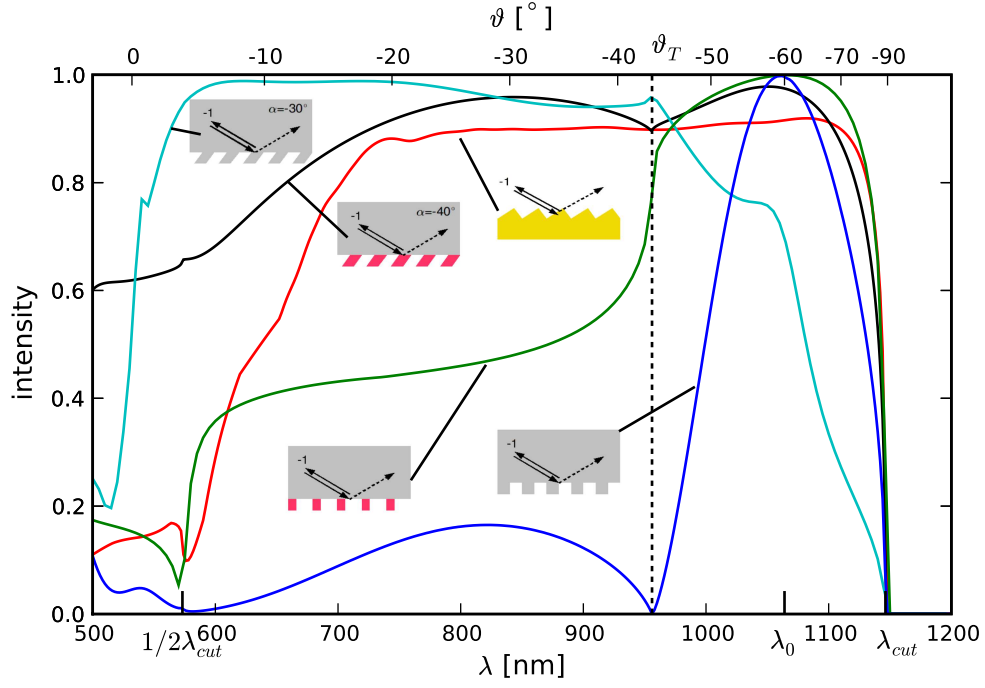


Fig. 3. Spectral characteristics of dielectric TIR gratings (*s*-polarized light), as compared to a best blazed gold grating with blaze angle 33° (*p*-polarized light). The blue line shows the result for a silica TIR grating with groove width $0.35T$ and depth $1.1T$, corresponding to maximum peak efficiency and spectral bandwidth (white circle in Fig.2(a)). The green line shows the spectral characteristics of a dielectric TIR grating featuring a high index material ($n = 2.4$) in the grating region ($w = 0.6T$, $d = 0.25T$, as marked by the white square in Fig.2(b)). The black line shows the spectral characteristics of a dielectric TIR grating with a high index material and slanted lamella ($\alpha = 40^\circ$), groove width $0.7T$, depth $0.5T$, corresponding to an optimal choice for large mean diffraction efficiency and simultaneously a comparably smooth spectrum, (white diamond in Fig.2(c)). The cyan line shows the result for a silica TIR grating with slanted lamella ($\alpha = 30^\circ$), groove width $0.3T$, depth $1.6T$, optimized for high short wavelengths efficiency.

The blue line in Fig.3 shows the spectral characteristics of the dielectric TIR grating, with width $0.35T$ and depth $1.1T$, in comparison to a best blazed gold grating (in air), with period $T = 614\text{nm}$, that has the same dispersion and incident angle as the TIR grating. The blaze angle of the gold grating was optimized to yield the largest possible bandwidth and peak efficiency in the given wavelength range, found as 33° . The dielectric TIR grating shows excellent properties in a 50-100nm band around its design wavelength. In particular, it reaches 100% diffraction efficiency at its design wavelength, and provides scattering losses smaller than -1dB (95% diffraction efficiency) over a bandwidth of 84nm. Here, it provides unsurpassed diffraction efficiency. Indeed, these high diffraction efficiencies cannot be reached with metallic gratings, whose inherent absorption inevitably results in losses [19]. However, as the wavelength is altered substantially from the design wavelength, the diffraction efficiency quickly drops to zero. In particular, as the angle of the -1^{st} diffraction order reaches the angle of total internal reflection between glass and air, the diffraction intensity drops to a sharp minimum, and for shorter wavelengths – corresponding to angles smaller than the angle of total internal reflection – the diffraction intensity does not recover its initially large value. These diffraction angles correspond to the case, when the -1^{st} diffraction order on the transmission side is no longer evanescent. However, a large diffraction intensity of the reflected -1^{st} order is not strictly forbidden at these scattering angles, as can be seen by the small but nonzero intensity value. This low diffraction efficiency over the largest part of the spectrum renders the TIR grating unusable for a large number of applications, including broadband pulse compression and most spectroscopic applications.

It is desirable, to resolve this issue, and to increase the spectral bandwidth of the TIR grating towards values that are comparable with metallic reflection gratings and dielectric transmission gratings, while maintaining the extraordinarily large peak diffraction efficiency, and the high resistance to laser induced damage. This is the first objective of this paper.

2. Large bandwidth dielectric TIR grating

The described phenomenon of a suppressed diffraction intensity at smaller angles, is remarkably robust. A first approach to increase the spectral bandwidth would be, to explore the landscape of possible combinations of the width and the depth, and to evaluate how this effects the spectral characteristics. However, the spectral bandwidth is only decreased. The lower panel of Fig.2(a) shows the -1dB spectral bandwidth as a function of the groove width and depth. It is seen, that the previous choice (with $w = 0.35T$ and $d = 1.1T$) corresponds already to the largest possible bandwidth, and for larger depths, the reflectivity and the bandwidth decrease in an oscillatory fashion. This behavior is understood qualitatively by referring to the theory of Kogelnik, who gave an estimate for the bandwidth $\Delta\lambda$ (full width at half maximum) of dielectric transmission gratings in the limit of deep grooves as

$$\frac{\Delta\lambda}{\lambda} = \frac{T}{d} \cot \vartheta_0. \quad (6)$$

It is seen, that indeed, the bandwidth is largest at small d .

This qualitative insight suggests already a way to improve the spectral characteristics of the grating. As an increase of the groove depth reduces the spectral bandwidth of the grating, one should try the opposite, one should decrease the groove depth. To do so, the difference of the propagation constants of the two modes in the grating region has to be enlarged, that is, the refractive index contrast has to be increased. Thus, in the grating region, we replace the glass by a material that has a larger refractive index. Suitable high index optical materials that are routinely available in the form of high quality thin films – through optical coating applications – are, e.g., Sapphire, diamond, TiO_2 , etc.. The latter two materials offer the largest refractive

index, around 2.4, in the wavelength range considered here [20]. From now on, we assume the refractive index of the high index material is 2.4. It should be noted, that the glass in the reflection region is kept. This is indeed important. If the material in the reflection region was changed together with the groove material, the grating period needed to be decreased accordingly. As a result, the entire computational problem was rescaled, such that no improvement was achieved.

The upper panel of Fig.2(b) shows the diffraction efficiency as a function of groove width and depth for the high index TIR grating. It is seen, that indeed, the first fringe is shifted towards shallower grooves. The smallest possible depth is achieved at around $w = 0.6T$ and $d = 0.25T$ (white square in Fig.2(b)). And indeed, here, the spectral bandwidth reaches its maximum (lower panel of Fig.2(b)). The green line in Fig.3 shows the corresponding spectral characteristics. The diffraction efficiency is increased over the entire spectrum as compared to the TIR grating based on glass. In particular, the $-1dB$ bandwidth around the design wavelength, is increased to 180nm, and is more than doubled as compared to the all-in-glass equivalent. Additionally, towards smaller wavelengths, in the range where the diffraction angle is larger than the angle of total internal reflection between glass and air, the diffraction efficiency is greater than 40%. This is a useful value for many spectroscopic applications. In addition, the moderate aspect ratio of the grating grooves (≈ 0.5), suggests that such a grating could be fabricated rather easily. Furthermore, the different nature of the grating and substrate material will probably help to fabricate structures with a very well defined depth, determined only by the thickness of the layer that is deposited prior to the etching process. The thickness of deposited layers can typically be controlled very accurately. Nevertheless, the natural question arises, whether this grating design can be further improved.

We have so far considered only the most simple of all grating profiles – rectangular grooves. It is well known that the diffraction efficiency of a gold grating – in particular its spectral characteristics – can be greatly improved, by choosing an appropriate blaze angle [19]. The blaze angle is chosen such that the incident beam and the diffracted beam are nearly perpendicular to the long face of the grating tooth (over the range of incident angles determined by the desired spectral range). Could the spectral characteristics of the TIR grating be further improved by using an equivalent geometry? As we will show below, the answer is yes, however, it is not sufficient to introduce a blaze, which becomes clear by considering the depth of the grooves necessary to accumulate the required phase shift in the grating region. As the geometry is more complex, the propagation constants of the waves vary in z -direction over the grating region, nevertheless, the mechanism for achieving maximum diffraction efficiency through the constructive interference of the fundamental and the first mode, is still qualitatively the same. And indeed, near 100% diffraction efficiency can be achieved with a large variety of groove geometries, such as symmetric triangles, asymmetric triangles, bow-ties, etc., by choosing a suitable width and depth. However, as is the case with rectangular grooves, generally a relatively large total depth is required, since the difference of the effective index of the propagation constants is never very large. E.g, in the case of symmetric triangles, a height of several T is required to achieve near 100% diffraction efficiency. In contrast, the blazed geometry is characterized by a small aspect ratio. In particular, the aspect ratio is smaller than $T/2$ (the blazed geometry is characterized by a triangle that features a right angle in its tip, related to the original ruling process that uses an inclined rectangular cutter). Because of this small aspect ratio, the blazed geometry cannot provide a high diffraction efficiency, for the type of dielectric gratings discussed here. However, a geometry that provides inclined faces, without sacrificing the possibility of a large groove depth, is the slanted geometry, characterized by rectangular lamella that are sheared along the periodic direction with a slant angle α . The slant angle is defined as the angle by which the groove wall is rotated as compared to the normal direction. Clockwise rotation corresponds to positive angles. Indeed, the slanted geometry has much in common with

the geometry of volume phase holographic gratings, where, in the general case, the crests of the holographically imprinted refractive index modulation are allowed to be slanted with respect to the grating normal (e.g. [7]).

To evaluate the diffraction characteristics of a slanted TIR grating, we compute the diffraction efficiency as a function of groove width, depth and wavelength for all slant angles $-90^\circ < \alpha < 90^\circ$, and for each slant angle, we evaluate the spectral bandwidth. The optimum slant angle is found as $\alpha = 40^\circ$. Fig.2(c) shows the plot (a movie sequence showing the plots for all α , is included in the supplemental material). The $-1dB$ bandwidth exceeds 300nm in a region around $w = 0.8T$, $d = 0.7T$. The black line in Fig.3 shows the corresponding spectral characteristics. This grating has a diffraction efficiency larger than 90% over nearly the full octave, and outperforms the best blazed gold grating over the largest part of the spectrum. In particular, two broad peaks of high diffraction efficiency appear, at around 30° , and at the design angle, 60° . These broad peaks overlap, and provide very high diffraction efficiency over the hole spectrum. Around each of the peaks, the spectrum is smooth. A shallow kink remains at the wavelength that corresponds to a diffraction angle equal to the angle of total internal reflection. This kink is at the origin of the jump that is observed in the width-depth map of the bandwidth, at the boundary of the region of large bandwidth. As the kink reaches above the $-1dB$ limit, the bandwidth jumps from a value characterized by the width of the right peak, to a value characterized by the width of both peaks together. It should be noted, that a combination of width and depth can be chosen, such that the kink between the two peaks at the angle of total internal reflection, disappears, and the spectrum becomes completely smooth over the full spectral range. However, in this case the spectral bandwidth is slightly smaller. Similarly, a width and depth can be chosen such that the right peak maintains 100% diffraction efficiency at the design wavelength, while the left peak is still higher than 80%. However, in this case, the kink becomes more pronounced. The result plotted here, represents a compromise between largest possible bandwidth and smoothness of the kink. Independent of that, it may also be interesting to operate this grating only with scattering angles smaller than the angle of total internal reflection, that is, the incident light enters the grating under a large angle, and the scattered light returns under angles smaller than the angle of total internal reflection. Thereby, only the left part of the spectrum was used. The design could then be optimized to yield highest efficiency specifically across the left peak.

The great improvement of the spectral characteristics provided by slanted lamella raises the question whether slanted lamella would also improve a single component TIR grating fabricated entirely from glass. As we will show now, the answer is yes, and it turns out that this is only achieved by optimizing the design in the way just described above, that is, by utilizing the left peak of the spectrum, while the right peak, at the design wavelength, remains small. This is indeed peculiar, because it means, that the grating does *not* feature high efficiency when the wavelength satisfies the Littrow condition, but at another wavelength, which also means, that one overlooks a highly efficient design, if one optimizes the grating parameters in the usual way at the design wavelength (because there the intensity is small). This is indeed remarkable. Recall the intuitive arguments that we put forward to explain why the Littrow configuration leads to a high efficiency. We considered the opposite case, when the incident wave is perpendicular to the surface, and the $+1^{st}$ and the -1^{st} diffraction order are aligned symmetrically around the surface normal. We argued, that, in this case, due to symmetry, the intensity of the orders must be equal, such that at maximum 50% diffraction efficiency can be achieved, and in contrast, if the grating is arranged in Littrow configuration, (near) 100% diffraction efficiency can be achieved. However, with the slanted geometry, the mirror symmetry of the grating around the surface normal is broken, and these arguments are no longer rigorously valid. It turns out that, for the slanted TIR grating in silica, this is indeed strongly violated, and the Littrow configu-

ration is no longer the universal optimum scattering geometry, rather, the optimum is achieved when the white light enters under a large angle, and the arc of diffracted beams leaves under small angles. To the best of our knowledge, an efficient grating with this type of scattering geometry has not been reported before.

Fig.2(d) shows the diffraction efficiency as a function of groove width and depth for the slanted silica TIR grating. As with the slanted high index TIR grating, we have evaluated the dependence of the diffraction characteristics on the slant angle (see second movie in the supplemental material), and present here the optimum, found with $\alpha = 30^\circ$. The largest bandwidth is found with width $w = 0.3T$ and depth $d = 1.6T$. The corresponding spectral characteristics are shown with a cyan line in Fig.3. The grating has excellent spectral characteristics for wavelength corresponding to diffraction angles below the angle of total internal reflection. For larger angles, the intensity falls off quickly, and at the design wavelength, it has already dropped below the $-1dB$ limit. This remarkable scattering geometry provides an unsurpassed diffraction efficiency over an almost 500nm band towards the short wavelength side of the spectrum. To the best of our knowledge, this represents again, the largest bandwidth highest efficiency reflection type optical grating devised so far.

3. Large bandwidth immersed grating

The described dramatic improvement of the spectral bandwidth of a dielectric TIR grating through a high index material, is more general. In particular, the introduction of a high index material improves dramatically also the performance of immersed dielectric gratings [21] at large incident angles. This is important, since, by virtue of Eq.5, large angles correspond to large dispersion. In addition, the immersed dielectric grating has been suggested previously, for providing a device that is easily cleaned, and usable in a rough (dirty) environment. Fig.1(b) shows the schematic of an immersed dielectric grating. The system is identical to the TIR grating, except that the air on the transmission side is replaced by a glass body. Besides the practical advantages related to cleaning, immersed dielectric gratings have another particular advantage over ordinary transmission gratings. In contrast to the latter, they can provide theoretically 100% diffraction efficiency. The latter is the topic of a recent paper [18], where the authors show, that 100% diffraction efficiency is linked to equal effective reflectivity of the top and bottom boundary of the grating region. If the incident and transmission halfspaces have a different refractive index – as is the case for an ordinary transmission grating, where the transmission region is air – the reflectivities of the top and bottom grating boundary are different, such that, even if an optimal interference condition is met for the two modes that travel in the grating region, a finite intensity remains, that results in an inevitable reflection loss into the ordinary reflected order. Thus, the diffraction efficiency is at best one minus an effective reflectivity of the optical grating. The latter can be substantial, especially when highest efficiencies are required, as is the case in many laser applications, and especially with large angles, where the grating provides its largest dispersion. In contrast, the immersed dielectric grating does not suffer this deficiency, and it can theoretically provide 100% diffraction efficiency – analog to the TIR grating.

However, as was the case with the TIR grating, the spectral bandwidth is limited, and, more importantly, if operated with large incident angles – corresponding to large dispersion –, the immersed grating starts to loose its extraordinarily good characteristics.

The four left panels of Fig.4 show the diffraction efficiency (s -polarization) as a function of groove width and depth, for a classical immersed dielectric grating illuminated under a large incident angle (throughout this section, we consider the same incident angle, $\vartheta_0 = 60^\circ$, and period, $T = 423.66\text{nm}$, as before, linked to the -1^{st} order Littrow condition, and providing the same dispersion). Four regimes appear. (1) At small groove depth, the ordinary transmitted

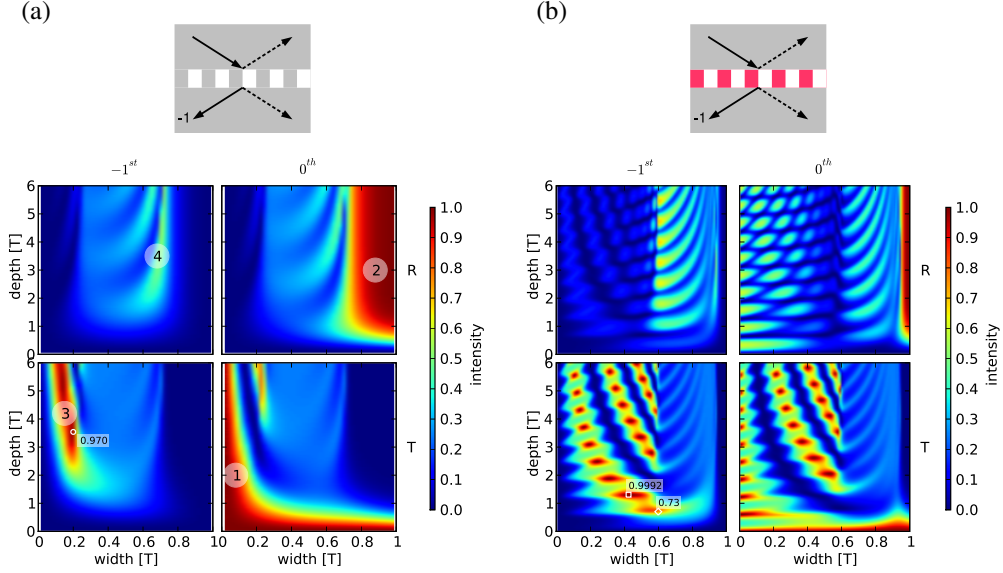


Fig. 4. (a) diffraction efficiency for an immersed dielectric grating, illuminated under a large incident angle ($\vartheta_0 = 60^\circ$). The upper panels show the reflected orders, the lower panels show the transmitted orders. The left and right panels show the -1^{st} and 0^{th} order, respectively. (b) same as in (a), for a grating featuring a high index material ($n = 2.4$) in the grating region.

intensity is large – the grating is negligible. (2) At large groove depth and large groove width, the ordinary reflected intensity is large – the grating region is increasingly similar to a large air gap, and total internal reflection occurs at the top grating surface. (3) Towards smaller groove widths, a region exists, where nearly all of the scattered intensity is scattered into the transmitted -1^{st} order – the grating resembles an efficient transmission grating. (4) Towards larger groove widths, a region exists, where a large part of the scattered intensity is scattered into the reflected -1^{st} order – the grating resembles a TIR grating. Thus, when illuminated with a large incident angle, depending on the groove width and depth, the immersed dielectric grating can be either more akin to a TIR grating or more akin to a transmission grating or somewhere in between. As a consequence of that, the regions of optimal choice of width and depth shrink to narrow domains, and generally, a high diffraction efficiency is achieved only at rather large depths, corresponding to aspect ratios that are not easily realized in practice. Qualitatively, the four regimes described above are a consequence of the effective refractive index experienced by the fundamental mode in the grating region, and the resulting reflectivities at the top and bottom boundary. The effective refractive index of the fundamental mode is determined by the mean refractive index. For large groove width, the mean refractive index is near to unity. Thus, as the incident angle is large, the fundamental mode in the grating region becomes evanescent. In this case, a notable amount of light can traverse the grating region only if the thickness of the grating is of the same order as the penetration depth of the evanescent wave. This small thickness conflicts with the interference condition for the two modes in the grating region, that requires a sufficiently large thickness to accumulate the necessary phase difference between the fundamental and the first mode. Thus, for those groove widths, for which the fundamental grating mode is evanescent, a high diffraction efficiency cannot be achieved. For large incident angles most of the reasonable choices for the width and depth fall into this regime. This makes the design of a high dispersion immersed grating a hard task.

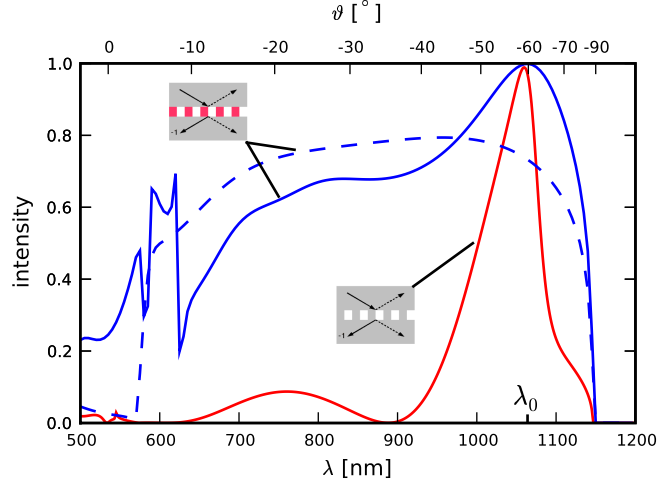


Fig. 5. Spectral characteristics for an immersed dielectric grating featuring a high index material in the grating region (blue lines), as compared to its all-in-glass equivalent (red line). The solid blue line represents a design that is optimized for highest peak efficiency, corresponding to $w = 0.43T$ and $d = 1.3T$, as shown by the white square in Fig.4(b)). The dashed blue line represents a design that is optimized for maximum bandwidth, corresponding to $w = 0.6T$ and $d = 0.7T$, as shown by the white diamond in Fig.4(b).

It is remarkable, that also here, the introduction of a high index material provides a solution, though, through a rather different mechanism then observed previously with the TIR grating. While, in case of the TIR grating, the high index material paved the way to a grating with shallow grooves, by providing a high refractive index contrast, here the high index material serves to increase the mean refractive index in the grating region – potentially above the refractive index of glass – to render the grating truly transparent for any incident angle (for most of the possible groove widths).

The four right panels of Fig.4 shows the diffraction efficiency of an immersed transmission grating using a high index material in the grating region (as before, we assume the refractive index of the high index material is $n = 2.4$). A region is opened up in the range $w < 0.6T$, where the grating becomes transparent. Near 100% diffraction efficiency is achieved with a number of possible choices of the width and depth. Fig.5 shows the spectral characteristics for two possible choices of the groove width and depth, as compared to the equivalent immersed grating fabricated entirely from glass. The solid blue line corresponds to $w = 0.43T$ and $d = 1.3T$, as shown by the white square in Fig.4(b), and represents a design that is optimized for highest peak efficiency in a narrow band around the design wavelength. The dashed blue line corresponds to $w = 0.6T$ and $d = 0.7T$, as shown by the white diamond in Fig.4(b), and represents a design that is optimized for maximum bandwidth (around 80% diffraction efficiency over nearly the full octave). To the best of our knowledge, the latter represents the largest bandwidth transmission grating (with the large dispersion considered here), devised so far.

4. Large bandwidth and 100% peak efficiency transmission grating in the classical scattering geometry

The successful improvement of the spectral and dispersive characteristics of a dielectric TIR, as well as dielectric immersed gratings, described in the preceding sections, intrigues the ques-

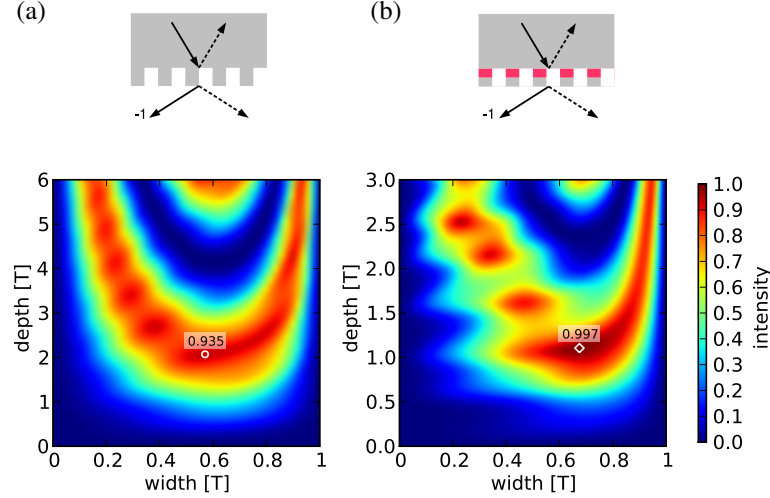


Fig. 6. (a) diffraction efficiency of a classical dielectric transmission grating. (b) diffraction efficiency of a double-layer grating featuring a buried high index layer, with thickness ratio $r = 0.5$. The circle and diamond mark those values of the groove width and depth, for which the spectral characteristics are evaluated in Fig.7.

tion, whether a high index material can also contribute to improve transmission gratings of the classical design.

Fig.1(c) shows the schematics of a classical transmission grating. As in the case of a dielectric TIR grating, light is diffracted at the back side of a glass body. However, here the incident angle is smaller than the angle of total internal reflection, such that the light is mainly scattered into transmitted diffraction orders. This grating geometry has a number of great advantages. (1) Due to refraction, the transmitted orders leave the grating under a large angle, which, in virtue of Eq.5 corresponds to large dispersion. Because of this, dielectric transmission gratings are typically superior over classical reflection gratings in the large dispersion regime (2) This is achieved without the need of a particularly small period, since, in virtue of Eq.4, the period is determined by the incident angle, and the latter is – again, due to the refraction – comparably small. This facilitates fabrication in practice (though, the period is not smaller than that of a gold grating with equal dispersion – it is the same). (3) The diffracted wave lives in air, saving the necessity to couple out the arc of diffracted rays through a flat or suitably curved glass-air interface (in certain applications, such as e.g. grism applications, the coupling out through a glass-air interface as faced in case of the TIR grating, may however also be used to a benefit, e.g., its dispersive nature may be specifically used to compensate for higher order dispersion [22]).

Because of these great advantages, the backside diffraction geometry is to date the primary choice for most dielectric grating applications.

Fig.6(a) shows the diffraction efficiency as a function of groove width and depth, for a classical dielectric transmission grating. The grating period $T = 614.30\text{nm}$, and the incident angle $\vartheta_0 = 36.67^\circ$ are chosen such that the diffraction angle of the transmitted -1^{st} order is 60° , such that both the diffraction angle and the angular dispersion are the same as before. The maximum diffraction efficiency is found with $w = 0.57T$ and $d = 2.07T$, on the center of the first fringe, as 93.5% (white circle). The red line in Fig.7 shows the corresponding spectral characteristics. The effective reflectivity of the top and bottom surface of the grating region are not equal, such that a reflection loss into the ordinary reflected order is encountered, and the diffraction

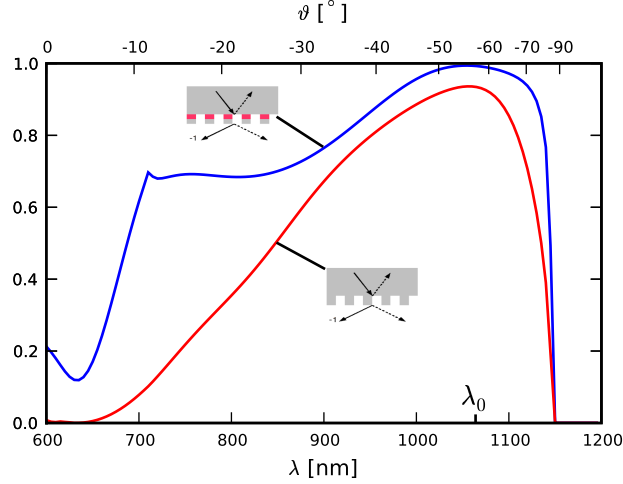


Fig. 7. Spectral characteristics of a dielectric transmission grating featuring a buried high index layer (blue line), as compared to a classical transmission grating (red line). The groove width and depth are $w = 0.68T$, $d = 1.1T$, respectively $w = 0.57T$, $d = 2.07T$, as marked by the diamond and circle in Fig.6.

efficiency remains smaller than 100%.

The qualitative understanding of the reflection loss suggests that a low loss into the fundamental reflected order could be achievable, if the effective refractive index in the grating region for the fundamental mode was close to $\sqrt{n^R}$, and the thickness of the grating region was close to an integer multiple of $\lambda/(4n^R)$, as is the principle of single layer anti-reflection coatings. In contrast, a large reflection loss into the fundamental order was expected, if the effective refractive index of the fundamental mode in the grating region was high. A substitution of the glass in the grating region by a high index material is therefore not promising. However it turns out that a simple double-layer grating is already enough. To ensure a low reflectivity at the bottom grating boundary, the high index grating layer is buried underneath a glass layer, as shown in Fig.6(b). To find the optimum thickness of both grating layers, we evaluated the diffraction efficiency as a function of width, depth and ratio $r = d_h/d_g$ of the thickness d_h and d_g of the high index layer, respectively the glass layer (third supplemental movie). Fig.6(b) shows the optimum choice corresponding to $r = 0.5$. The optimum width and depth is found as $w = 0.68T$ and $d = 1.1T$. Remarkably, the grating reaches effectively 100% diffraction efficiency. Thus, the TIR grating featuring a buried high index layer is indeed a complementary approach to a transmission grating featuring 100% diffraction efficiency, and an alternative to the immersed dielectric grating devised in [18]. Additionally, the spectral characteristics are greatly improved. The blue line in Fig.7 shows the spectral characteristics. The grating surpasses a classical transmission grating over the entire spectrum. To the best of our knowledge, this represents the largest bandwidth, high efficiency transmission grating devised to date.

5. Summary and conclusions

We have analyzed the diffraction characteristics of dielectric gratings that feature a high index grating layer, and shown parameter choices that are superior in terms of bandwidth and efficiency. A qualitative understanding is supplied in combination with rigorous calculations. The common grating types were considered, including reflection gratings, immersed transmis-

sion gratings and classical transmission gratings. Several profile types were explored, including novel structures that comprise a combination of enhanced material and enhanced geometry. The suggested devices are within current manufacturing capabilities. The gratings are compared to existing technology and applications are pointed out. We expect these types of gratings to become a useful addition to the existing range of grating geometries.

Acknowledgements

H.R. would like to thank Frieder Mugele for reserving him the freedom and time that allowed him to do this work. We are grateful to Detlef Lohse for providing us access to his computer cluster, on which most of the calculations were performed.